

## MIT Open Access Articles

*Theoretical ingredients of a Casimir analog computer*

The MIT Faculty has made this article openly available. **Please share** how this access benefits you. Your story matters.

**Citation:** Rodriguez, A. W., A. P. McCauley, J. D. Joannopoulos, and S. G. Johnson. "Theoretical ingredients of a Casimir analog computer." *Proceedings of the National Academy of Sciences* 107, no. 21 (May 25, 2010): 9531-9536.

**As Published:** <http://dx.doi.org/10.1073/pnas.1003894107>

**Publisher:** National Academy of Sciences (U.S.)

**Persistent URL:** <http://hdl.handle.net/1721.1/80336>

**Version:** Final published version: final published article, as it appeared in a journal, conference proceedings, or other formally published context

**Terms of Use:** Article is made available in accordance with the publisher's policy and may be subject to US copyright law. Please refer to the publisher's site for terms of use.



# Theoretical ingredients of a Casimir analog computer

Alejandro W. Rodriguez<sup>a</sup>, Alexander P. McCauley<sup>a</sup>, John D. Joannopoulos<sup>1,a</sup>, and Steven G. Johnson<sup>b</sup>

<sup>a</sup>Department of Physics and <sup>b</sup>Department of Mathematics, Massachusetts Institute of Technology, Cambridge, MA 02139

Contributed by John D. Joannopoulos, March 24, 2010 (sent for review February 12, 2010)

**We derive a correspondence between the contour integration of the Casimir stress tensor in the complex-frequency plane and the electromagnetic response of a physical dissipative medium in a finite real-frequency bandwidth. The consequences of this correspondence are at least threefold: First, the correspondence makes it easier to understand Casimir systems from the perspective of conventional classical electromagnetism, based on real-frequency responses, in contrast to the standard imaginary-frequency point of view based on Wick rotations. Second, it forms the starting point of finite-difference time-domain numerical techniques for calculation of Casimir forces in arbitrary geometries. Finally, this correspondence is also key to a technique for computing quantum Casimir forces at micrometer scales using antenna measurements at tabletop (e.g., centimeter) scales, forming a type of analog computer for the Casimir force. Superficially, relationships between the Casimir force and the classical electromagnetic Green's function are well known, so one might expect that any experimental measurement of the Green's function would suffice to calculate the Casimir force. However, we show that the standard forms of this relationship lead to infeasible experiments involving infinite bandwidth or exponentially growing fields, and a fundamentally different formulation is therefore required.**

Casimir forces arise due to quantum fluctuations of the electromagnetic field (1–4) and can play a significant role in the physics of neutral, macroscopic bodies at micrometer separations, such as in new generations of micro-electromechanical systems (5, 6). These forces have previously been studied both in delicate experiments at micron and submicron length scales (7–10) and also in theoretical calculations that are only recently becoming feasible for complex nonplanar geometries (11–22). Theoretical efforts to predict Casimir forces for geometries very unlike the standard case of parallel plates have begun to yield fruit, having demonstrated a number of interesting results for strong-curvature structures (17, 23–29). But theoretical challenges still remain, more so in geometries involving multiple bodies and/or multiple length scales (14).

In this paper, we describe a correspondence between the calculation of Casimir forces for vacuum-separated objects and a similar electromagnetic-force calculation in which the objects are instead separated by a conducting fluid, as illustrated in Fig. 1. The requirement that the geometry be mapped in this fashion is a practical consideration for any calculation based on the time domain (real frequencies). In fact, it is the theoretical *equivalent* of a crucial and well-known technique for accurate numerical evaluation of Casimir forces, in which the force integrand is deformed via contour integration and commonly evaluated over the imaginary-frequency axis (2, 14). Our formulation circumvents difficulties with all previous expressions of Casimir forces in terms of frequency integrals of classical Green's functions, which required either formally infinite bandwidth (when evaluated over real frequencies) or exponentially growing fields (when evaluated over imaginary frequencies)—instead, we exploit the moderate-bandwidth real-frequency response of a physical, dissipative system. We believe that this mathematical equivalence between complex contour mappings and physical dielectric deformations reveals unique opportunities for the experimental and theoretical study of Casimir interactions. On the theoretical side, this correspondence makes it easier to understand Casimir systems from

the perspective of conventional classical electromagnetism, based on real-frequency responses, in contrast to the standard point of view based on Wick rotations (imaginary frequencies). Furthermore, it has already led to a finite-difference time-domain numerical method for calculation of Casimir forces in arbitrary geometries and materials (30, 31).

In this paper, we focus on the derivation of this correspondence along with a third application of that idea: a technique for calculation of Casimir forces based on experimental *S*-matrix (microwave antenna) measurements in centimeter-scale models. Note that an experiment (centimeter-scale model) of the sort proposed here is not a Casimir “simulator,” in that one is not measuring forces but rather a quantity that is mathematically related to the Casimir force—in this sense, it is an *analog computer*. The use of tabletop models and analog computers in physics, though previously unexplored in the context of quantum vacuum fluctuations, continues to play an important role in contemporary research areas like quantum evolution (32) and quantum information (33). For example, many analog computers have been developed to simulate fluid flow problems (34, 35), electromagnetic and acoustic wavefields (36), cell electrolysis (37), and many of the problems governed by Laplace's equations (38). More recently, advances in the field of microwave electromagnetics (which offers unprecedented control over sources and detection of microwaves), have spurred the development of classical electromagnetic analog computations for studying complex quantum problems, including the calculation of the energy levels of Bloch electrons in magnetic fields (39) and the dynamics of certain classes of chaotic quantum systems (32), to name a few. Computing fluctuation-induced effects like the Casimir force is substantially different from previous analog-computation problems in quantum simulation, in that it involves not the evolution of a single quantum state but rather the combined effect of fluctuations over a broad (formally infinite) bandwidth.

In what follows, we describe the step-by-step conceptual development of an analog computer for calculation of Casimir forces. The first section reviews a well known formulation of the Casimir-force problem, in which the Casimir force is expressed in terms of an integral of the classical Green's function (GF) via the electromagnetic stress tensor (ST) and the fluctuation-dissipation theorem (2). Although numerical constraints normally require integration over either the real or imaginary-frequency axes, we abandon both of these standard choices and instead consider mappings over the general complex-frequency ( $\omega$ ) plane. The following section derives an equivalence between the complex-frequency GF (the GF evaluated over a complex-frequency contour) of a geometry and the real-frequency (standard) GF of an identical geometry with a transformed electromagnetic medium  $\epsilon_c$ . This correspondence is a way to realize this contour-deformation technique in a real experiment. From this point of view, it becomes clear that only certain contours in the complex-frequency plane correspond to physically realizable  $\epsilon_c$  and that neither the real or imaginary-frequency axes are suitable

Author contributions: A.W.R., J.D.J., and S.G.J. designed research; A.W.R. and A.P.M. performed research; A.W.R. and S.G.J. contributed new reagents/analytic tools; A.W.R., A.P.M., J.D.J., and S.G.J. analyzed data; and A.W.R. and S.G.J. wrote the paper.

The authors declare no conflict of interest.

<sup>1</sup>To whom correspondence should be addressed. E-mail: joannop@mit.edu.

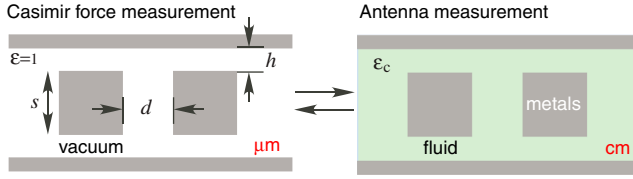


**Fig. 1.** Schematic illustration of correspondence between two methods of calculating Casimir forces. (Left): Numerical method requiring evaluation of the force integrand over the imaginary-frequency axis (or some suitable complex-frequency contour). (Right): Antenna (*S*-matrix) measurements of the electromagnetic response at tabletop (e.g., centimeter) length scales. Here, the effect of a contour deformation is achieved by a material deformation that corresponds to the presence of a conductive fluid between the objects.

for experiments (the latter due to the fact that it is equivalent to a gain medium). Instead, we identify a suitable contour whose response is equivalent to a physically realizable, conventional conducting medium. The *Numerical Experiment* section demonstrates that the response of such a medium yields the correct Casimir force by performing numerical experiments on the geometry shown in Fig. 1 and then goes on to describe the properties of the corresponding integrand. Finally, we consider the implications of the above mapping for practical experiments, including possible materials, length scales, and sources of experimental errors. The key point is that, once the Casimir force is expressed in terms of the response of a realizable medium over a reasonably narrow bandwidth, the scale invariance of Maxwell's equations permits this response to be measured at any desired length scale, e.g., in a tabletop microwave experiment.

### Casimir Force via Stress Tensor

The Casimir force can be expressed as an integral of the mean electromagnetic ST over all frequencies (2). The mean ST is determined simply from the classical GF (the fields in response to current sources at a fixed frequency), a consequence of the fluctuation-dissipation theorem. It turns out, however, that this frequency integral is badly behaved from the perspective of numerical calculations (or experiments, below). In particular, the integral is formally infinite, requiring regularization, and highly oscillatory. Fortunately, because the integrand is analytic, one can deform the integration contour into the complex-frequency  $\omega$  plane. More generally, given an arbitrary contour  $\omega(\xi)$  (conveniently parameterized by a real  $\xi$ ), the force in the *i*th coordinate direction is given by

$$F_i = \text{Im} \int_0^\infty d\xi \frac{d\omega(\xi)}{d\xi} \int_{\text{surface}} \sum_j \langle T_{ij}(\mathbf{r}, \omega(\xi)) \rangle dS_j. \quad [1]$$

The standard Wick rotation corresponds to the particular choice  $\omega(\xi) = i\xi$  and yields a smooth and rapidly decaying integrand (14). The mean ST  $\langle T_{ij} \rangle$  is related to the electric ( $\mathbf{E}$ ) and magnetic ( $\mathbf{H}$ ) field correlation functions by the standard equation (assuming nonmagnetic materials,  $\mu = 1$ , for simplicity):

$$\langle T_{ij}(\mathbf{r}, \omega) \rangle = \langle H_i(\mathbf{r})H_j(\mathbf{r}) \rangle - \frac{1}{2} \delta_{ij} \sum_k \langle H_k(\mathbf{r})H_k(\mathbf{r}) \rangle + \varepsilon(\mathbf{r}, \omega) \left[ \langle E_i(\mathbf{r})E_j(\mathbf{r}) \rangle - \frac{1}{2} \delta_{ij} \sum_k \langle E_k(\mathbf{r})E_k(\mathbf{r}) \rangle \right]. \quad [2]$$

The field correlation functions are, in turn, related to the frequency-domain classical photon GF,  $G_{ij}(\omega; \mathbf{r}, \mathbf{r}')$ , by the fluctuation-dissipation theorem:

$$\langle E_i(\mathbf{r})E_j(\mathbf{r}') \rangle = \frac{\hbar}{\pi} \omega^2 G_{ij}(\omega; \mathbf{r}, \mathbf{r}'), \quad [3]$$

$$\langle H_i(\mathbf{r})H_j(\mathbf{r}') \rangle = -\frac{\hbar}{\pi} (\nabla \times)_{i\ell} (\nabla' \times)_{jm} G_{\ell m}(\omega; \mathbf{r}, \mathbf{r}'), \quad [4]$$

where  $G_{ij}$  satisfies Maxwell's equations:

$$[\nabla \times \nabla \times - \varepsilon(\mathbf{r}, \omega)\omega^2] \mathbf{G}_j(\omega; \mathbf{r}, \mathbf{r}') = \delta(\mathbf{r} - \mathbf{r}') \hat{\mathbf{e}}_j. \quad [5]$$

Eq. 5 can be solved in a number of ways, for example, by a finite-difference discretization (14) or even analytically in one dimension (2). Of course, the diagonal ( $\mathbf{r}' = \mathbf{r}$ ) part of the GF is formally infinite, but this singularity is not relevant because its surface integral is zero, and it is typically removed by some regularization (e.g., by the finite discretization or by a finite antenna size in the proposed experiments below). A crucial step for evaluation of Eq. 1, as mentioned above, is the passage to imaginary frequencies  $\omega(\xi) = i\xi$ . For real frequencies  $\omega(\xi) = \xi$ , the GF is oscillatory, leading to a highly oscillatory ST integrand that does not decay—even when a regularization (ultraviolet cutoff) is imposed, integrating a highly oscillatory function over a broad bandwidth is problematic. When evaluated over imaginary frequencies, on the other hand, the GF is exponentially decaying, due to the operator in [5] becoming positive-definite ( $\nabla \times \nabla \times + \varepsilon\xi^2$ ) (14), leading to a decaying nonoscillatory integrand.

However, the Wick rotation is not the only contour in the complex plane that leads to a well-behaved decaying integrand. This idea is illustrated by Fig. 2, which shows the force integrand in the complex plane for the piston-like geometry of Fig. 1, recently shown to exhibit nonmonotonic variations in the force as a function of plate separation  $h$  (14, 26). In particular, we calculate the (*x*-direction) force integrand  $dF_x/d\omega = \int_{\text{surf}} \sum_j T_{xj}(\mathbf{r}, \omega) dS_j$  on one square, for  $h = 0.5d$  and  $s = d$ , where  $d$  is the separation between the blocks. Here, we plot  $\ln |\Re dF_x/d\omega|$ , which illustrates the basic features of the integrand  $d\omega/d\xi dF_x/d\omega$  (whereas  $\text{Im} dF_x/d\omega$  also contributes to the total force, it is qualitatively similar and therefore omitted). As described above, this integrand is oscillating along the  $\Re \omega$  axis and decaying along the  $\text{Im} \omega$  axis. Moreover, it also decays along any contour where  $\text{Im} \omega$  is increasing (such as the three contours shown, to be considered in more detail below).

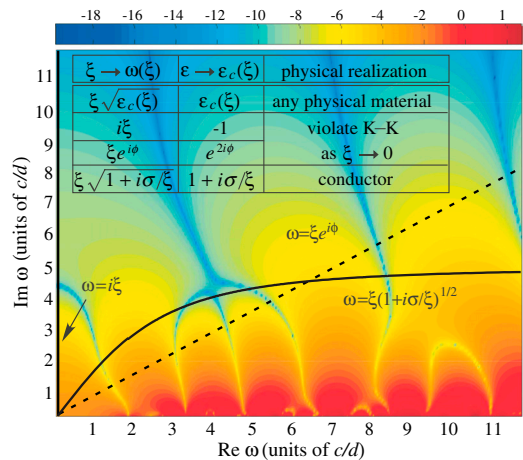


**Fig. 2.** Complex-frequency  $\omega$  plot of the Casimir-force integrand ( $\ln |\Re dF_x/d\omega|$ ), where  $dF_x/d\omega$  is in units of  $\hbar/d^2$ , for the geometry of Fig. 1. As the real- $\omega$  axis is approached, the integrand becomes highly oscillatory, which is only partially revealed here because of the finite frequency resolution. Various integration contours of interest are labeled as black and dashed lines. (Inset): Vacuum  $\varepsilon = 1$  contour deformations  $\omega(\xi)$  and their corresponding (real frequency) physical realizations  $\varepsilon_c(\xi)$ .

## Correspondence

The fact that  $\omega$  and  $\varepsilon$  appear together in [5], as  $\varepsilon\omega^2$ , immediately suggests that, instead of changing  $\omega$  via a complex mapping  $\omega(\xi)$  (again parametrized by real  $\xi$ ), we can instead operate at real  $\xi$  by transforming  $\varepsilon$ . Specifically, evaluating [5] over a complex contour  $\omega(\xi)$  is formally equivalent to evaluating [5] over real frequencies  $\omega(\xi) = \xi$ , but for a complex dielectric permittivity given by

$$\varepsilon_c(\mathbf{r}, \xi) = \frac{\omega^2(\xi)}{\xi^2} \varepsilon(\mathbf{r}, \omega(\xi)). \quad [6]$$

Thus, given a medium  $\varepsilon(\mathbf{r}, \omega)$  and a complex-frequency contour  $\omega(\xi)$  over which we wish to compute the ST, we can transform to an equivalent problem involving a real-frequency ST evaluated over a complex dielectric  $\varepsilon_c(\mathbf{r}, \xi)$ , determined by [6]. [Conversely, the GF of any frequency-dependent material  $\varepsilon_c(\xi)$  at a given point in space can be related to the GF for vacuum ( $\varepsilon = 1$ ) at that point by going from the real frequency  $\xi$  to a complex frequency  $\omega = \xi\sqrt{\varepsilon_c(\xi)}$ .] Eq. 6 yields an intuitive explanation for why transforming to the complex-frequency plane is numerically advantageous: Complex-frequency deformations correspond to lossy materials that act to damp out the frequency oscillations. Furthermore, this equivalence is also of practical value to Casimir-force calculations (beyond being of pedagogical value): First, it forms an essential ingredient of a numerical finite-difference time-domain method, formulated in ref. 30 and demonstrated for various geometries in ref. 31. The other application, discussed below, involves the possibility of computing the force via real experiments (in contrast to numerical experiments), in the spirit of analog computations.

## Complex-Frequency Green's Functions via Correspondence

Because the Casimir ST is expressed in terms of the electromagnetic GF, and the GF of a system at microwave length scales is merely a rescaling of the GF of the system at micron length scales\*, one can conceivably measure the GF (electric field in response to a current source) in an experiment via the  $S$ -matrix elements of antennas at centimeter scales and in doing so determine the Casimir force via integration of the ST. The passage to complex frequencies is essential to an experiment, as in numerics, because measuring the GF in the original geometry  $\varepsilon(\mathbf{r}, \xi)$  (real frequency  $\xi$ ), as the electromagnetic response to an oscillating current source  $\sim e^{i\xi t}$ , will yield narrow peaks in its spectrum, requiring integration of a highly oscillatory force integrand over an infinite bandwidth and thus imposing significant experimental challenges. Thus, one would like a way to *implement* the effect of complex-frequency deformations in an experiment, which is the subject of the remaining text.

There are at least three ways to obtain the complex-frequency GF  $G_{ij}(\mathbf{r}, \mathbf{r}', \omega)$  of a geometry  $\varepsilon(\mathbf{r}, \omega)$  in an experiment [the electric field  $\mathbf{E}(\mathbf{r})$  at a point  $\mathbf{r}$  in response to a dipole current source  $\mathbf{J} = \delta(\mathbf{r} - \mathbf{r}')e^{-i\omega t}$ , evaluated at *complex frequency*  $\omega = \omega(\xi)$ ]: First, one may directly measure the electromagnetic field in response to a current source with time dependence  $\sim e^{-i\omega(\xi)t}$  [the most straightforward interpretation of complex-frequency GFs (2)]. However, an  $\omega(\xi)$  in the upper-half complex plane corresponds to both sources and fields with exponential growth in time, which is difficult for experiments. A second possibility involves measuring the standard real-frequency GF (the response to an oscillating source  $e^{-i\xi t}$ ) over a large frequency bandwidth and

then performing a *numerical analytic continuation* of the form  $\xi \rightarrow \omega(\xi)$ . However, it is already known that inferring the Casimir force from real- $\omega$  GF measurements is extremely difficult, requiring the GF over a very wide bandwidth to a high accuracy (14). A third alternative, and the subject of this paper, is to instead exploit the correspondence above, in order to measure the real-frequency GF (the response to an oscillating source  $\sim e^{-i\xi t}$ ) of a physical medium with a complex permittivity given by [6]. As noted above, due to the presence of loss [corresponding to the imaginary part of  $\omega(\xi)$ ], the integrand will be both smooth and decaying as a function of real-frequency  $\xi$ .

In order for this approach to be experimentally viable,  $\varepsilon_c$  must satisfy two properties: It should correspond to an  $\omega$  contour where the ST integrand is rapidly decaying, and it should be physically realizable. For simplicity, we begin by considering complex contours for a geometry in which the objects are separated by vacuum, so that the ST need only be evaluated in vacuum ( $\varepsilon = 1$ ). This choice implies that, at those points where the ST needs to be evaluated, the real-frequency medium corresponding to a contour-deformation  $\omega(\xi)$  is determined by a dielectric function of the form  $\varepsilon_c(\xi) = \omega(\xi)^2/\xi^2$ .

We begin by noting that, in order for  $\varepsilon_c(\xi)$  to correspond to a physical medium, it must satisfy the complex-conjugate property  $\varepsilon_c(-\xi) = \varepsilon_c(\xi)^*$  as well as the Kramers–Kronig (K–K) relations (40). It is most important to satisfy these conditions for small  $\xi$ , because the ST integrand is dominated by long-wavelength contributions. One should also prohibit gain media, which would lead to the exponentially growing fields we are trying to avoid by not using sources with complex  $\omega$ . For example, a Wick rotation corresponds to a medium with dispersion  $\varepsilon_c(\xi) = -1$ , and this is only possible at  $\xi = 0$  in a gain medium, because in a dissipative medium,  $\varepsilon_c$  is real and positive along the whole imaginary- $\omega$  axis (this is implied by K–K). The generalization to arbitrary rotations in the complex plane  $\varepsilon = e^{2i\phi}$  yields similar difficulties, because these both act as gain media and also violate  $\varepsilon_c(-\xi) = \varepsilon_c(\xi)^*$  near  $\xi = 0$ . Thus, no realizable material can emulate these standard contours even in a narrow bandwidth around  $\xi = 0$ , as summarized in Table 1 (also shown in the *Inset* of Fig. 2).

Although traditional Wick rotations correspond to unphysical materials (as argued in the preceding paragraph), there are obviously many physical lossy materials to choose from, each of which corresponds to a contour in the complex plane, and one merely needs to find such a “physical” contour on which the ST is rapidly decaying so that experiments can be performed over reasonable bandwidths. A simple and effective lossy material for this purpose is a conductor with conductivity  $\sigma$ . Because the integral will turn out to be dominated by the contributions near zero frequency, it is sufficient to consider  $\sigma$  to be a constant (the dc conductivity), although of course the full experimental permittivity  $\varepsilon_c(\xi)$  could also be used. Specifically, we consider the general class of conductors defined by dispersion relations of the form  $\varepsilon_c(\xi) = 1 + i\sigma/\xi$ , corresponding to vacuum with a complex contour  $\omega_\sigma(\xi) = \xi\sqrt{1 + i\sigma/\xi}$ . As shown in Fig. 2, the integrand of this contour is in fact well behaved, rapidly decaying and exhibits few oscillations. Moreover, because conductive fluids are ubiquitous, this choice is especially promising for experiments (see the section on analog computations).

**Table 1. Vacuum  $\varepsilon = 1$  contour deformations  $\omega(\xi)$  and their corresponding (real frequency) physical realizations  $\varepsilon_c(\xi)$**

$\xi \rightarrow \omega(\xi)$	$\varepsilon \rightarrow \varepsilon_c(\xi)$	Physical realization
$\xi\sqrt{\varepsilon_c(\xi)}$	$\varepsilon_c(\xi)$	Any physical material
$i\xi$	$-1$	Violate K-K as $\xi \rightarrow 0$
$\xi e^{i\phi}$	$e^{2i\phi}$	
$\xi\sqrt{1 + i\sigma/\xi}$	$1 + i\sigma/\xi$	Conductor

\*The invariance of the GF to changes in length scale is a consequence of the scale invariance of Maxwell's equations for geometries composed of perfect-metal objects. When either the perfect-metal approximation breaks down or real materials are involved, changing the length scale of the problem also requires an appropriate dielectric rescaling—i.e., materials with the appropriate dielectric response at the relevant length scales.

### Numerical Experiment

We now consider the Casimir force for the same structure as in Fig. 1, still calculated by the same finite-difference method as in Fig. 3, but we now focus on the properties along different contour choices for both physical and unphysical media. In particular, Fig. 2 (Top) plots the partial integral  $\int_0^\xi (d\omega/d\xi)(dF_x/d\omega)d\xi$ , normalized by the total force  $\int_0^\infty dF_x$ , as a function of  $\xi$ . [As it must, the total integral over  $\xi$ , the force  $F_x$ , is invariant regardless of the contour  $\omega(\xi)$  and agrees with previous results (14); specifically,  $F_x = 0.0335 (\hbar c/d^3)$ ]. We now comment on two important features of the  $\omega_\sigma$  contour that are relevant to experiments.

First, the Jacobian factor for  $\omega_\sigma$  is given by  $d\omega_\sigma/d\xi = 0.5(2 + i\sigma/\xi)/\sqrt{1 + i\sigma/\xi}$  and turns out to be very important at low  $\xi$ . The ST integrand itself goes to a constant as  $\xi \rightarrow 0$  (due to the constant contribution of zero-frequency modes), but the Jacobian factor diverges in an integrable square-root singularity  $\sim \sqrt{\sigma/\xi}$ . Because this singularity is known analytically, however, separate from the measured or calculated GF, integrating it accurately poses no challenge. Second, the larger the value of  $\sigma$ , the more rapidly the ST integrand decays with  $\xi$ , and as a consequence the force integral for larger  $\sigma$  is dominated by smaller  $\xi$  contributions. In comparison, previous calculations of Casimir forces along the imaginary-frequency axis revealed that the relevant  $\xi$  bandwidth was determined by some characteristic length scale of the geometry such as body separations (14). Here we have introduced an additional parameter  $\sigma$  that can squeeze the relevant  $\xi$  bandwidth into a narrower region. This “spectral squeezing” effect is potentially useful for experiments, because it partially decouples the experimental length scale of the geometry from the required frequency bandwidth.

### A Casimir Analog Computer

As a consequence of the above results, we can now outline a possible experiment at centimeter length scales that determines the Casimir force at micron length scales, a Casimir analog computer (CAC). Suppose that one wishes to compute the Casimir force between perfect-metal objects separated by vacuum, such as the geometry in Fig. 1. One would then construct a scale model of this geometry at a tabletop scale (e.g., centimeters) out of metallic objects (which can be treated as perfect metals at microwave and longer wavelengths). To determine the ST integrand along a complex- $\omega_\sigma$  contour, one would measure the GF at real-frequencies  $\xi$  for the model immersed in a conducting fluid. The GF is related to the  $S$  matrix of pairs of antennas, and the diagonal of the GF to the  $S$ -matrix diagonal of a single antenna (noting that the finite size of the antenna automatically regularizes the integrand, as noted after [5]). It is important for the model structure to be large enough that the introduction of a small dipole-like antenna does not significantly alter the electromagnetic response. In general, the ST must be integrated in space over a closed surface around the object, and correspondingly the antenna’s  $S$ -matrix spectrum must be measured at a number of antenna positions (two-dimensional quadrature points) around this surface. (Unless one is interested in computing the force on a single atom, which requires a single antenna measurement.) The different components of the GF tensor correspond to different antenna orientations. The magnetic GF can be determined from the photon GF by [3] or possibly by employing “magnetic dipole” antennas formed by small current loops.

We now consider a particular CAC (at the centimeter scale) that employs realistic geometric and material parameters. Many available fluids exhibit almost exactly the desired material properties from above. One such example is saline water, which has  $\epsilon(\xi) = \epsilon_s + i\sigma/\xi$ , where  $\epsilon_s \approx 80$  and  $\sigma \approx 5$  S/m for relatively small values of salt concentration (41). A calculation using these parameters, based on the geometry of Fig. 1, assuming object sizes and separations at the centimeter to meter scale (we choose  $d = 0.3$  m for the structure in Fig. 1, corresponding to a fre-

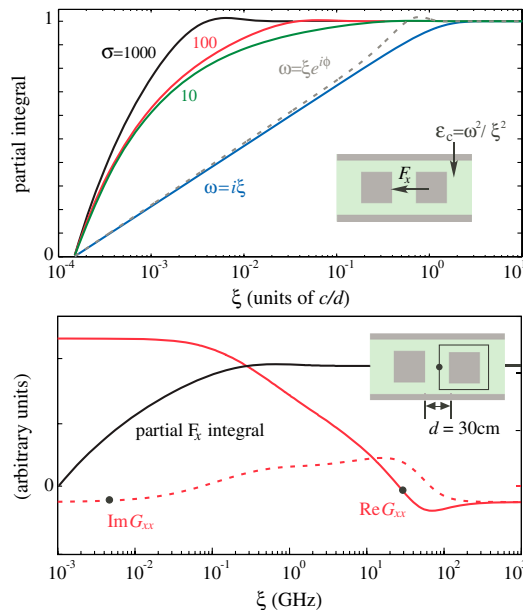


**Fig. 3.** (Top): Partial force integral  $\int_0^\xi dF_x$ , normalized by  $F_x$ , as a function of  $\xi$ , for the various  $\omega(\xi)$ -contours (equivalently, various  $\epsilon_c = \omega^2/\xi^2$ ) shown in Fig. 3. The solid green, red, and black lines correspond to conductive media with  $\sigma = 10, 10^2$ , and  $10^3$ , respectively ( $\sigma$  has units of  $c/d$ ). The dashed gray and solid blue lines correspond to  $\phi = \pi/4$  and  $\phi = \pi/2$  (Wick) rotations, respectively. (Bottom): Illustration of the required frequency bandwidth for a possible realization using saline solution at separation  $d = 30$  cm. The red lines plot the  $xx$  component of the photon GF  $G_{xx}$  at a single location on the surface contour (see Inset) as a function of  $\xi$  (GHz). The black line is the corresponding partial force integrand.

quency of 1 GHz), reveals that it is only required to integrate the stress tensor up to small GHz frequencies  $\xi$ , which is well within the reach of conventional antennas and electronics. This idea is illustrated in Fig. 3 (Bottom), which plots the  $G_{xx}$  component of the GF (Red Lines) as well as the partial force integrand (Black Line), showing the high  $\xi < 1$  GHz cancellations that occur once the ST is integrated along a surface (Inset). We note that most salts exhibit additional dispersion for  $\xi > 10$  GHz (41), but we do not need to reach those frequency scales. (Nevertheless, should there be substantial dispersion in the conducting fluid, one could easily take it into account as a different complex- $\omega$  contour.)

Some attention to detail is required in applying this correspondence correctly. For instance, by using network analyzers, what is measured in such an experiment is not the photon GF  $\mathbf{G}$  but rather the electric  $S$  matrix  $\mathbf{S}^E$  (the currents in a set of receiver antennas due to currents in the source antennas), related to the electric GF (the  $\mathbf{E}$ -field response to an electric current  $\mathbf{J}$ ) by a factor depending on the antenna geometry alone (relating  $\mathbf{J}$  to  $\mathbf{E}$ ). The electric GF will differ from the photon GF by a factor of the real-frequency  $i\xi$ . To summarize, the photon GF will be given in terms of the measured  $\mathbf{S}^E$  by  $G_{ij}(\omega) = (\alpha/i\xi)S_{ij}^E(\xi)$ , where  $\alpha$  is the antenna-dependent geometric factor (which can be measured with high accuracy). To obtain the ST from  $G_{ij}$ , one multiplies by factors of  $\omega(\xi)^2$  as in [3]. Fig. 3 (Bottom) illustrates the expected behavior of  $S_{xx} \sim G_{xx}/\xi$  in a realistic system employing a saline solution with  $d = 30$  cm.

We believe that such an experiment is feasible and capable of yielding accurate Casimir forces. In particular, the accuracy of the resulting force would only be limited by the magnitude of any measurement error, because the remaining postprocessing steps can be performed with very high accuracy using well known techniques (14). With respect to measurement errors, we believe these to be well within the bounds necessary to obtain forces with

accuracies better than or similar to those of our previous (and current) numerical experiments (14, 26, 28, 30, 31, 42). Some of these may include: electronic noise, finite-size effects associated with any measurement device (e.g., antenna width), and surface roughness. It should be possible to make surface roughness negligible at centimeter scales, and in any case roughness is present in real Casimir experiments and is known to have a small effect if the roughness amplitude is small compared to the surface separations (43, 44) (although roughness could be intentionally introduced in the microwave system to study its effect). Finite-size effects are expected to be small because they are closely analogous to the effect of discretization in our numerical simulations (which give a finite size to current sources, among other effects), which do not contribute significantly to the force if the finite size is small enough. Specifically, if  $a$  is a typical length scale in the problem (here, centimeters), for resolutions = 50 pixels/ $a$ , corresponding to a smallest representable length scale of  $0.02a$ , we obtain at least 1% accuracy in the force. For a tabletop experiment with  $a$  around 10 cm, this corresponds to antenna sizes  $<2$  mm, which is easily achievable. One must also deal with electronic sources of noise in the microwave regime. These sources include interference effects coming from sources in the vicinity of the experiment as well as thermal noise, both of which become significant at frequencies above 100 MHz (45). There are, however, many effective standard ways to reduce interference errors, such as shielding and grounding of the entire apparatus (46). Finally, though insignificant in the microwave regime, one may encounter noise originating in the receiver circuit, e.g., shot and pink noise. These absolute noise floors scale as the measurement bandwidth and can therefore be reduced if these measurements are performed over smaller frequency ranges (equivalent to averaging) (45). Fortunately, both of these sources of noise are independent of the power at which one operates the antenna (measurement) device—therefore, because the GF measurement upon which this experiment is based is independent of the source amplitude (within the limits of the linear response of the materials), it is possible to increase the source power in order to significantly reduce the signal-to-noise ratio. For example, typical network analyzers can yield noise in the range (95, 120) dB at these frequencies for powers in the milliwatts range (45), which is negligible even when accumulated over hundreds of measurements in a random walk. Moreover, numerical methods have the same sort of noise in the form of accumulated round-off error, which is also on the order of  $10^{-9}$  or larger [proportional to machine precision multiplied by the condition number of the matrix (47)], and we have not observed any appreciable effect of such round-off noise on the accuracy (which is mostly limited by discretization/finite-size effects).

## Conclusion

The calculation of Casimir forces and other fluctuation-induced interactions presents a challenge for both theory and experiment (3, 8, 48, 49). Especially for three-dimensional geometries, tabletop experiments offer an alternative route to rapidly exploring many different geometric configurations that are only now starting to become accessible to conventional numerical calculation (although complex geometries involving many objects remain challenging). Although many details of such an experiment remain to be developed, we believe that the basic ingredients are both clear and feasible, at least when restricted to perfect-metal bodies. The most difficult case to realize seems to be the force between imperfect-metal or dielectric bodies with a permittivity  $\epsilon(\omega)$ , because the corresponding tabletop system requires materials

with a specified dispersion relation  $\epsilon_c^{\text{body}}(\xi)/\epsilon_c^{\text{fluid}}(\xi) = \epsilon(\omega(\xi))$  relative to the conducting fluid. This may be an opportunity for specially designed metamaterials with the desired frequency response. Analog computations at large length scales should also enable scientists to study Casimir forces in geometries composed of real dielectrics whose low-frequency response is of interest, such as recent predictions of repulsive forces between dielectric and magnetic (50–52) or magnetoelectric (53, 54) bodies which currently only exist at long wavelengths (55).

The correspondence (developed here) between complex-frequency deformations of the ST and causal material transformations is an indispensable ingredient for the development of a CAC. However, this equivalence is useful in at least two other ways: First, it is being used to design numerical methods for Casimir-force calculations based on the finite-difference time-domain method (30, 31); second, it offers an alternative perspective on the Casimir effect. Specifically, one of the difficulties involved in understanding Casimir forces comes from the wide-bandwidth aspect of the real-frequency domain, which makes it impossible to separate contributions coming from individual electromagnetic modes and therefore discourages the use of ideas from standard classical electromagnetism based on geometric or material resonances. For example, electromagnetic metamaterials are commonly designed to have effective materials properties that differ dramatically from their constituent materials, but only over a narrow bandwidth because they rely on strong resonant effects in subwavelength structures (56). Physicists familiar with Casimir theory typically consider the Casimir-force contributions decomposed along the imaginary-frequency axis, where the contributions are exponentially decaying and are mostly nonoscillatory because they are far removed from the resonant modes (all of which lie below the real-frequency axis) (3, 4, 14). However, this viewpoint is foreign to most researchers from the classical electromagnetism community, which focuses on real frequencies and is often concerned with ideas based on geometric or material resonances in narrow bandwidths. The imaginary-frequency viewpoint indicates that resonant effects on Casimir phenomena are weak and that broad real- $\omega$  bandwidths are important to Casimir interactions, but this insight is far removed from the classical photonics way of thinking. On the other hand, absorption loss is well understood and familiar in classical electromagnetism, so our theoretical framework may provide a gentler pathway into Casimir physics from classical electromagnetics research: By realizing that Casimir forces are determined by a narrow-bandwidth response to a system with artificial dissipation added everywhere, it becomes immediately clear even from the classical-photonics viewpoint why strong resonance effects are damped out. For example, although metamaterials can be designed to have effective materials properties that differ dramatically from their constituent materials over a narrow bandwidth, the fact that these effects mostly disappear at imaginary frequencies (57) can be difficult to convey to traditional metamaterials researchers. At the same time, it is a familiar fact in the metamaterial community that useful metamaterial properties are rapidly overwhelmed as strong dissipation is added to the system, and by expressing Casimir interactions in these terms more familiar classical analytical tools become applicable.

**ACKNOWLEDGMENTS.** We are grateful to Zheng Wang and Peter Shor at Massachusetts Institute of Technology for useful discussions. This work was supported by the Army Research Office through the Institute for Soldier Nanotechnology under Contract W911NF-07-D-0004, the Massachusetts Institute of Technology Ferry Fund, and by Department of Energy Grant DE-FG02-97ER25308 (to A.W.R.).

1. Casimir HBG (1948) On the attraction between two perfectly conducting plates. *Proc K Ned Akad Wetensch* 51:793–795.
2. Lifshitz EM, Pitaevskii LP (1980) *Statistical Physics: Part 2* (Pergamon, Oxford).
3. Milonni PW (1993) *The Quantum Vacuum: An Introduction to Quantum Electrodynamics* (Academic, San Diego).

4. Buhmann SY, Welsch D-G (2007) Dispersion forces in macroscopic quantum electrodynamics. *Prog Quant Electron* 31:51–130.
5. Serry FM, Walliser D, Jordan MG (1998) The role of the Casimir effect in the static deflection of and stiction of membrane strips in microelectromechanical systems MEMS. *J Appl Phys* 84:2501–2506.

6. Chan HB, Aksyuk VA, Kleinman RN, Bishop DJ, Capasso F (2001) Quantum mechanical actuation of microelectromechanical systems by the Casimir force. *Science* 291:1941–1944.
7. Bordag M, Mohideen U, Mostepanenko VM (2001) New developments in the Casimir effect. *Phys Rep* 353:1–205.
8. Milton KA (2004) The Casimir effect: Recent controversies and progress. *J Phys A-Math Gen* 37:R209–R277.
9. Lamoreaux SK (2005) The Casimir force: Background, experiments, and applications. *Rep Prog Phys* 68:201–236.
10. Capasso F, Munday JN, Iannuzzi D, Chan HB (2007) Casimir forces and quantum electrodynamic torques: Physics and nanomechanics. *IEEE J Sel Top Quant* 13:400–415.
11. Emig T, Hanke A, Golestanian R, Kardar M (2001) Probing the strong boundary shape dependence of the Casimir force. *Phys Rev Lett* 87:260402.
12. Gies H, Langfeld K, Moyaerts L (2003) Casimir effect on the worldline. *J High Energy Phys* 6:18.
13. Gies H, Klingmuller K (2006) Worldline algorithms for Casimir configurations. *Phys Rev D* 74:045002.
14. Rodriguez A, Ibanescu M, Iannuzzi D, Joannopoulos JD, Johnson SG (2007) Virtual photons in imaginary time: Computing Casimir forces in arbitrary geometries via standard numerical electromagnetism. *Phys Rev A* 76:032106.
15. Rahi SJ, Emig T, Jaffe RL, Kardar M (2008) Casimir forces between cylinders and plates. *Phys Rev A* 78:012104.
16. Rahi SJ, et al. (2008) Nonmonotonic effects of parallel sidewalls on Casimir forces between cylinders. *Phys Rev A* 77:030101(R).
17. Emig T, Graham N, Jaffe RL, Kardar M (2007) Casimir forces between arbitrary compact objects. *Phys Rev Lett* 99:170403.
18. Dalvit DA, Neto Mia PA, Lambrecht A, Reynaud S (2008) Proving quantum-vacuum geometrical effects with cold atoms. *Phys Rev Lett* 100:040405.
19. Kenneth O, Klich I (2008) Casimir forces in a T-operator approach. *Phys Rev B* 78:014103.
20. Reynaud S, Neto Maia PA, Lambrecht A (2008) Casimir energy and geometry: Beyond the proximity force approximation. *J Phys A Math Theor* 41:164004.
21. Reid MTH, Rodriguez AW, White J, Johnson SG (2009) Efficient computation of three-dimensional Casimir forces. *Phys Rev Lett* 103:040401.
22. Pasquali S, Maggs AC (2009) Numerical studies of Lifshitz interactions between dielectrics. *Phys Rev A* 79:020102(R).
23. Emig T, Jaffe RL, Kardar M, Scardicchio A (2006) Casimir interaction between a plate and a cylinder. *Phys Rev Lett* 96:080403.
24. Gies H, Klingmuller K (2006) Casimir edge effects. *Phys Rev Lett* 97:220405.
25. Bordag M (2006) Casimir effect for a sphere and a cylinder in front of a plane and corrections to the proximity force theorem. *Phys Rev D* 73:125018.
26. Rodriguez A, et al. (2007) Computation and visualization of Casimir forces in arbitrary geometries: Non-monotonic lateral-wall forces and failure of proximity force approximations. *Phys Rev Lett* 99:080401.
27. Miri M, Golestanian R (2008) A frustrated nanomechanical device powered by the lateral Casimir force. *Appl Phys Lett* 92:113103.
28. Rodriguez AW, et al. (2008) Stable suspension and dispersion-induced transition from repulsive Casimir forces between fluid-separated eccentric cylinders. *Phys Rev Lett* 101:190404.
29. Milton KA, Parashar P, Wagner J, Pelaez C (2009) Multiple scattering Casimir force calculations: Layered and corrugated materials, wedges, and Casimir-Polder forces. *J Vac Sci Technol B* 28:C4A8–C4A16.
30. Rodriguez AW, McCauley AP, Joannopoulos JD, Johnson SG (2009) Casimir forces in the time domain: Theory. *Phys Rev A* 80:012115.
31. McCauley AP, Rodriguez AW, Joannopoulos JD, Johnson SG (2010) Casimir forces in the time domain: Applications. *Phys Rev A* 81:012119.
32. Lu W, Rose M, Pance K, Sridhar S (1999) Quantum resonances and decay of a chaotic fractal repeller observed using microwaves. *Phys Rev Lett* 82:5233.
33. Lloyd S (2008) Quantum information matters. *Science* 319:1209–1211.
34. Norum VD, M Adelberg, Farrenkopf RL (1962) *Analog Simulation of Particle Trajectories in Fluid Flow* (Association for Computing Machinery, New York), pp 235–254.
35. Onega RJ (1971) Analog computer solution of the electrodiffusion equation for a simple membrane. *Am J Phys* 40:390–394.
36. Cirjanic BM (1971) A practical field plotter using a hybrid analog computer. *IEEE Trans Ind Electron* IECI-18:16–20.
37. Martin RJ, Masnari NA, Rowe JE (1960) Analog representation of Poisson's equation in two dimensions. *IRE Trans Electronic Comp* EC-9:490–496.
38. Karplus W (1958) *Analog Simulation: Solution of Field Problems* (McGraw-Hill, New York), pp 1–434.
39. Kuhl U, Stockmann HJ (1997) Microwave realization of the Hofstadter butterfly. *Phys Rev Lett* 80:3232.
40. Jackson JD (1998) *Classical Electrodynamics* (Wiley, New York), 3rd Ed, pp 1–790.
41. Klein LA, Swift CT (1977) An improved model for the dielectric constant of sea water at microwave frequencies. *IEEE Trans Antenn Propag* 25:104–111.
42. Rodriguez AW, Joannopoulos JD, Johnson SG (2008) Repulsive and attractive Casimir forces in a glide-symmetric geometry. *Phys Rev A* 77:062107.
43. Bezerra VB, Klimchitskaya GL, Romero C (2000) Surface roughness contribution to the Casimir interaction between an isolated atom and a cavity wall. *Phys Rev A* 61:022115.
44. Neto Maia PA, Lambrecht A, Reynaud S (2005) Roughness correction to the Casimir force: Beyond the proximity force approximation. *Europhys Lett* 69:924.
45. Pozar DM (2004) *Microwave Engineering* (Wiley, New York), 3rd Ed.
46. Morrison R (2007) *Grounding and Shielding* (Wiley, New York).
47. Trefethen LN, Bau D (1997) *Numerical Linear Algebra* (SIAM, Philadelphia), 1st Ed.
48. Genet C, Lambrecht A, Reynaud S (2008) The Casimir effect in the nanoworld. *Eur Phys J-Spec Top* 160:183–193.
49. Klimchitskaya GL, Mohideen U, Mostapanenko VM (2009) The Casimir force between real materials: experiment and theory. *Rev Mod Phys* 81:1827–1885.
50. Boyer TH (1968) Quantum electrodynamic zero-point energy of a conducting spherical shell and the Casimir model for a charged particle. *Phys Rev* 174:1764.
51. Milton KA, DeRaad LL, Jr, Schwinger J (1978) Casimir self-stress on a perfectly conducting spherical shell. *Ann Phys* 115:388.
52. Yannopoulos V, Vitanov NV (2009) First-principles study of Casimir repulsion in metamaterials. *Phys Rev Lett* 103:120401.
53. Zhao R, Zhou J, Economou EN, Soukoulis CM (2009) Repulsive Casimir force in chiral metamaterials. *Phys Rev Lett* 103:103602.
54. GRushin AG, Cortijo A (2010) Tunable Casimir repulsion with three-dimensional topological insulators. arXiv:1002.3481.
55. Gadenne M (2002) *Optical Properties of Nanostructured Random Media* (Springer, Berlin).
56. Ziolkowski RW (2006) *Metamaterials: Physics and Engineering Explorations* (Wiley, New York).
57. Rosa FSS (2009) On the possibility of Casimir repulsion using metamaterials. *J Phys Conf Series* 161:012039.